RESEARCH ARTICLE OPEN ACCESS

Spatial-Temporal Patterns of β-Amyloid Accumulation

A Subtype and Stage Inference Model Analysis

Lyduine E. Collij, PhD, Gemma Salvadó, PhD, Viktor Wottschel, PhD, Sophie E. Mastenbroek, MSc, Pierre Schoenmakers, BSc, Fiona Heeman, MSc, Leon Aksman, PhD, Alle Meije Wink, PhD, Bart N.M. Berckel, PhD, MD, Wiesje M. van de Flier, PhD, Philip Scheltens, PhD, MD, Pieter Jelle Visser, PhD, MD, Frederik Barkhof, PhD, MD, Sven Haller, PhD, MD, Juan Domingo Gispert, PhD, and Isadora Lopes Alves, PhD, for the Alzheimer's Disease Neuroimaging Initiative; for the ALFA study

Correspondence
Dr. Collij
l.collij@amsterdamumc.nl

Neurology® 2022;98:e1692-e1703. doi:10.1212/WNL.0000000000200148

Abstract

Background and Objectives

β-amyloid (Aβ) staging models assume a single spatial-temporal progression of amyloid accumulation. We assessed evidence for Aβ accumulation subtypes by applying the data-driven Subtype and Stage Inference (SuStaIn) model to amyloid-PET data.

Methods

Amyloid-PET data of 3,010 participants were pooled from 6 cohorts (ALFA+, EMIF-AD, ABIDE, OASIS, and ADNI). Standardized uptake value ratios were calculated for 17 regions. We applied the SuStaIn algorithm to identify consistent subtypes in the pooled dataset based on the cross-validation information criterion and the most probable subtype/stage classification per scan. The effects of demographics and risk factors on subtype assignment were assessed using multinomial logistic regression.

Results

Participants were mostly cognitively unimpaired (n = 1890 [62.8%]), had a mean age of 68.72 (SD 9.1) years, 42.1% were *APOE* ε4 carriers, and 51.8% were female. A 1-subtype model recovered the traditional amyloid accumulation trajectory, but SuStaIn identified 3 optimal subtypes, referred to as frontal, parietal, and occipital based on the first regions to show abnormality. Of the 788 (26.2%) with strong subtype assignment (>50% probability), the majority was assigned to frontal (n = 415 [52.5%]), followed by parietal (n = 199 [25.3%]) and occipital subtypes (n = 175 [22.2%]). Significant differences across subtypes included distinct proportions of *APOE* ε4 carriers (frontal 61.8%, parietal 57.1%, occipital 49.4%), participants with dementia (frontal 19.7%, parietal 19.1%, occipital 31.0%), and lower age for the parietal subtype (frontal/occipital 72.1 years, parietal 69.3 years). Higher amyloid (Centiloid) and CSF p-tau burden was observed for the frontal subtype; parietal and occipital subtypes did not differ. At follow-up, most participants (81.1%) maintained baseline subtype assignment and 25.6% progressed to a later stage.

Discussion

Whereas a 1-trajectory model recovers the established pattern of amyloid accumulation, SuStaIn determined that 3 subtypes were optimal, showing distinct associations with Alzheimer disease risk factors. Further analyses to determine clinical utility are warranted.

RELATED ARTICLE

Editorial
Multiple Cortical to Striatal Accumulation Trajectories of β-Amyloid: Do All Roads Lead to Rome?
Page 695

From the Department of Radiology and Nuclear Medicine (L.E.C., V.W., S.E.M., P.S., F.H., A.M.W., B.N.M.B., F.B., I.L.A.), Alzheimer Center and Department of Neurology (W.M.v.d.F., P.S., P.J.V.), and Department of Epidemiology & Data Science (W.M.v.d.F.), Amsterdam UMC, Vrije Universiteit Amsterdam, the Netherlands; BarcelonaBeta Brain Research Center (BBRC) (G.S., J.D.G.), Pasqual Maragall Foundation; IMIM (Hospital del Mar Medical Research Institute) (G.S., J.D.G.), Barcelona, Spain; Stevens Neuroimaging and Informatics Institute (L.A.), Keck School of Medicine, University of Southern California, Los Angeles; Centre for Medical Image Computing and Queen Square Institute of Neurology (F.B.), UCL, UK; Faculty of Medicine of the University of Geneva (S.H.); CIMC–Centre d'Imagerie Médicale de Cornavin (S.H.), Genève, Switzerland; Department of Surgical Sciences, Radiology (S.H.), Uppsala University, Sweden; Department of Radiology (S.H.), Beijing Tiantan Hospital, Capital Medical University, Beijing, China; and Centro de Investigación Biomédica en Red de Bioingeniería, Biomateriales y Nanomedicina (CIBER-BBN) (J.D.G.), Madrid, Spain.

Go to Neurology.org/N for full disclosures. Funding information and disclosures deemed relevant by the authors, if any, are provided at the end of the article. The Article Processing Charge was funded by the authors.

Data used in preparation of this article were obtained from the Alzheimer's Disease Neuroimaging Initiative (ADNI) database (adni.loni.usc.edu). As such, the investigators within the ADNI contributed to the design and implementation of ADNI and/or provided data but did not participate in analysis or writing of this report. A complete listing of ADNI investigators can be found in the coinvestigators list at links.lww.com/WNL/B862.

ALFA coinvestigators are listed at links.lww.com/WNL/B863.

The Article Processing Charge was funded by the authors.

Glossary

Aβ = β-amyloid; **ABIDE** = Alzheimer's biomarkers in daily practice project; **AD** = Alzheimer disease; **ADNI** = Alzheimer's Disease Neuroimaging Initiative; **ALFA** = Alzheimer's and Family cohort of the Barcelonaβeta Brain Research Center; **CAA** = cerebral amyloid angiopathy; **CL** = Centiloid; **CU** = cognitively unimpaired; **CVIC** = cross-validation information criterion; **DLB** = dementia with Lewy bodies; **EMIF-AD** = European Medical Information Framework for AD; **MCI** = mild cognitive impairment; **MLR** = multinomial logistic regression; **MMSE** = Mini-Mental State Examination; **MNI** = Montreal Neurological Institute; **OASIS** = Open Access Series of Imaging Studies; **pi** = postinjection; **PiB** = Pittsburgh compound B; **ROI** = region of interest; **SuStaIn** = Subtype and Stage Inference; **SUVR** = standard uptake value ratio.

PET imaging is one of the main tools to study amyloid pathology in vivo. The technique makes use of β-amyloid (Aβ) radiotracers validated against neuropathology.[1-3] In comparison with other Aβ biomarkers, such as CSF or plasma, PET imaging provides spatial-temporal information,[4] which may be of particular interest for Alzheimer disease (AD) research and clinical trials.

Since the first proposal of a population-based neuropathologic progression scheme by Braak and Braak in 1991,[5] multiple amyloid PET studies have proposed similar frameworks that would allow the staging of an individual's biomarker along a spectrum of pathologic burden.[6-9] These approaches have demonstrated high applicability at the population level and indicate that determining the extent of amyloid pathology can be used to better characterize prognosis and risk of cognitive decline.[7-9] However, these models have invariably relied on the assumption that the path to AD dementia–like levels of Aβ is the same across individuals, disregarding variability in the data that could point to distinct trajectories of amyloid accumulation. On the other hand, most studies aimed at identifying disease subtypes assume participants to be at a common disease stage (e.g., dementia) for valid comparison,[10] which is especially challenging in a sporadic and long-term disease process such as AD. Therefore, although both approaches are useful, stage-only models do not disentangle potential subtypes, and subtype-only models do not account for distinct stages across individuals, hampering the identification of the simultaneous effect of subtypes and stages on disease presentation and risk assessment.[11]

Recently, a data-driven method has been developed to jointly resolve both stages and subtypes from heterogeneous cross-sectional data, namely the Subtype and Stage Inference (SuStaIn) model.[11] This algorithm was applied previously to uncover patterns of brain atrophy in AD, showing an improved prediction of clinical conversion compared to stage- or subtype-only models.[11] More recent work identified 4 distinct spatiotemporal phenotypes of tau accumulation, which were associated with different clinical profiles and longitudinal cognitive outcomes, suggesting the value of such models for improving individualized prognosis and clinical care.[13] In the context of amyloid, previous descriptions of a homogeneous spatial-temporal progression of amyloid pathology were not in full agreement,[4] and staging models' success could be attributed to a reduced spatial resolution (i.e., small number of stages covering large portions of the brain).[8,9] Therefore, it is possible that an underlying heterogeneity in amyloid spatial-temporal progression remains unresolved.

To determine whether there is evidence for patterns of cerebral Aβ accumulation, we applied the SuStaIn model to pooled amyloid-PET data from 5 cohorts. These included observational cohorts and open-access data repositories with mostly cognitively unimpaired individuals and clinical populations with different levels of cognitive impairment. We first assessed whether subtypes of progression are statistically preferred to the common assumption of a universal trajectory. We then described possible subtype differences with respect to main demographics and risk factors. Finally, we validated the observed subtypes in a longitudinal subset of data.

Methods

Cohorts

All participants from 5 cohorts with available amyloid PET scans of sufficient quality for quantification were retrospectively included (Table 1). [^{18}F]Flutemetamol scans of 358 cognitively unimpaired (CU) participants from the Alzheimer's and Family cohort of the Barcelonaβeta Brain Research Center (ALFA)[14] and 190 CU participants from the Innovative Medicine Initiative European Medical Information Framework for AD (EMIF-AD)[15] were included. [^{18}F]Florbetaben scans of 350 memory clinic patients from the Alzheimer's biomarkers in daily practice project (ABIDE) were included.[16] A total of 572 [^{11}C]Pittsburgh compound B (PiB) and 360 [^{18}F]florbetapir scans of CU participants were obtained from the Open Access Series of Imaging Studies–3 (OASIS) dataset.[17] A total of 1,180 participants scanned with [^{18}F]florbetapir were included from the Alzheimer's Disease Neuroimaging Initiative (ADNI) database. The ADNI study was launched in 2003 as a public–private partnership, led by principal investigator Michael W. Weiner, MD. The primary goal of ADNI is to test whether serial MRI, PET, other biological markers, and clinical and neuropsychological assessment can be combined to measure the progression of mild cognitive impairment (MCI) and early AD.

In total, the complete dataset available for this study consisted of amyloid PET imaging data from 3,010 participants (1890

Table 1 Baseline Demographics for Each Cohort

	[18F]Flutemetamol		[18F]Florbetaben			[11C]PiB			[18F]Florbetapir							
			ABIDE (n = 350)			OASIS (n = 572)			OASIS (n = 360)			ADNI (n = 1,180)				
	ALFA (n = 358), CU	EMIF-AD (n = 190), CU	CU (n = 126)	Cognitively impaired (n = 66)	Dementia (n = 158)	CU (n = 482)	Cognitively impaired (n = 32)	Dementia (n = 58)	CU (n = 304)	Cognitively impaired (n = 25)	Dementia (n = 31)	Missing (n = 27)	CU (n = 430)	Cognitively impaired (n = 525)	Dementia (n = 198)	Total (n = 3,010)[a]
Age, y	61.50 (4.64)	70.44 (7.55)	60.53 (7.80)	66.13 (7.09)	66.68 (7.34)	64.63 (9.32)	70.44 (8.35)	74.09 (8.21)	66.78 (8.51)	70.92 (6.30)	73.50 (6.84)	72.72 (9.84)	73.97 (6.78)	72.87 (7.96)	75.02 (7.75)	68.72 (9.06)
Sex, F	220 (61.5)	112 (58.9)	54 (42.9)	24 (36.4)	65 (41.1)	292 (60.6)	18 (56.3)	24 (41.4)	163 (53.6)	17 (68.0)	19 (61.3)	14 (51.9)	233 (54.2)	222 (42.3)	82 (41.4)	1,559 (51.8)
MMSE	29.18 (0.95)	28.99 (1.14)	27.77 (2.40)	26.94 (2.01)	23.12 (4.09)	29.13 (1.15)	27.97 (1.94)	23.77 (6.01)	29.04 (1.26)	28.56 (1.53)	24.45 (4.07)	26.00 (2.55)	29.06 (1.19)	28.02 (1.78)	22.49 (3.28)	27.88 (2.93)
***APOE* ε4 carriership +[b]**	198 (55.3)	62 (33.3)	49 (38.9)	31 (47.0)	83 (52.5)	161 (33.5)	15 (46.9)	35 (60.3)	101 (34.7)	7 (30.4)	23 (74.2)	8 (36.4)	124 (29.0)	241 (45.9)	129 (65.5)	1,267 (42.1)
***APOE* ε2 carriership +[c]**	31 (8.7)	17 (8.9)	15 (11.9)	9 (13.6)	12 (7.6)	81 (16.8)	4 (12.5)	6 (10.3)	52 (17.9)	3 (13.0)	2 (6.5)	1 (4.5)	57 (13.3)	52 (9.9)	8 (4.1)	350 (11.6)
Centiloid	2.76 (17.02)	14.58 (23.02)	13.00 (26.53)	28.35 (32.36)	45.51 (45.15)	11.77 (26.70)	36.75 (43.74)	72.14 (42.55)	18.77 (32.06)	47.02 (59.19)	75.70 (42.30)	39.71 (39.32)	17.79 (27.89)	33.45 (35.89)	60.43 (35.33)	24.24 (35.75)
Aβ positivity[d]	38 (10.6)	40 (21.1)	29 (23.0)	29 (43.9)	101 (63.9)	90 (18.7)	14 (43.8)	49 (84.5)	85 (28.0)	13 (52.0)	27 (87.1)	15 (55.6)	125 (29.1)	275 (52.4)	167 (84.3)	1,097 (36.4)
CSF $A\beta_{42}$	1,309.38 (371.89)	892.28 (317.98)	1,078.08 (283.21)	906.45 (319.25)	745.72 (298.79)	NA			NA			NA	1,246.92 (433.15)	1,016.95 (431.53)	696.12 (338.48)	NA
CSF p-tau	16.44 (7.49)	76.34 (44.38)	53.98 (29.84)	65.75 (27.82)	70.90 (33.08)	NA			NA			NA	22.13 (9.35)	26.60 (14.32)	36.71 (16.37)	NA
CSF essay	Elecsys	Adx Euroimmun	Innotest			NA			NA				Elecsys			

Abbreviations: Aβ = β-amyloid; ABIDE = Alzheimer's biomarkers in daily practice project; AD = Alzheimer disease; ADNI = Alzheimer's Disease Neuroimaging Initiative; ALFA = Alzheimer's and Family cohort of the Barcelonaβeta Brain Research Center; CU = cognitively unimpaired, including both controls and subjective cognitive decliners; EMIF-AD = European Medical Information Framework for AD; MMSE = Mini-Mental State Examination; OASIS = Open Access Series of Imaging Studies; PiB = Pittsburgh compound B.
Cognitively impaired participants had a clinical diagnosis of mild cognitive impairment or a Clinical Dementia Rating of 0.5 (in the absence of a clinical diagnosis). Dementia includes both AD and non-AD. Values are mean (SD) or n (%).
[a] 1890 CU, 648 cognitively impaired, 445 dementia, 27 missing.
[b] Participant carries at least 1 *APOE* ε4 allele.
[c] Participant carries at least 1 *APOE* ε2 allele.
[d] Aβ positivity = >21 Centiloid.

CU, 648 cognitively impaired, 445 dementia, and 27 with missing diagnosis at time of baseline PET). Participants labeled as cognitively impaired had a clinical diagnosis of MCI or a Clinical Dementia Rating score of 0.5 in the absence of a clinical diagnosis. In addition, from cohorts where longitudinal PET imaging was available (ADNI and OASIS), we selected those for whom a second scan was performed ≥4 years after baseline (n = 519).

Standard Protocol Approvals, Registrations, and Patient Consents

The protocol, patient information, consent form, and other relevant study documentation were approved by the ethics committees or institutional review boards of each site before study initiation. The studies were performed in accordance with the Declaration of Helsinki and consistent with Good Clinical Practice. Before enrollment, all patients provided written informed consent.

Image Acquisition and Processing

[^{18}F]Flutemetamol scans from the ALFA cohort consisted of 4 frames (4 × 5 minutes) acquired 90–110 minutes postinjection (pi). Images were checked for motion and PET and accompanying structural T1-weighted MRI were warped into Montreal Neurological Institute (MNI) space using SPM12. [^{18}F] Flutemetamol EMIF-AD scans were acquired using a dual-time-window protocol[18] (0–30 minutes pi, 60 minutes break, 90–110 minutes pi), but only the late frames (90–110 minutes pi) were used for this work.[19] [^{18}F]Florbetaben scans from ABIDE were processed as described previously, with static scans consisting of 4 frames (4 × 5 minutes) acquired 90–110 minutes pi.[19] All EMIF-AD and ABIDE images were checked for motion and accompanying structural T1-weighted magnetic resonance images were coregistered to PET using Vinci software (Max Planck Institute for Neurologic Research) and then warped into MNI using SPM12. [^{18}F]Florbetapir (50–70 minutes pi) and [^{11}C]PiB (30–60 minutes pi) data from the OASIS platform were processed with FreeSurfer and the PET Unified Pipeline.[20] Finally, [^{18}F]florbetapir PET scans from ADNI consisted of 4 frames (4 × 5 minutes), acquired 50–70 minutes pi, and were processed using FreeSurfer.

PET Quantification

For all cohorts, standard uptake value ratios (SUVRs) relative to the cerebellar gray matter were available for all Desikan-Killiany atlas regions.[21] For the purposes of this work, a set of 17 regions of interest (ROIs) was constructed by volume-weighted averaging of anatomically adjacent regions. The final 17 regions were as follows: anterior, posterior, and isthmus cingulate; medial and lateral orbitofrontal; precuneus; inferior, middle, and superior frontal; supramarginal; insula and lingual gyrus; the lateral parietal lobe (superior and inferior parietal); lateral temporal lobe (middle, transverse, and superior temporal, superior temporal sulcus, and temporal pole); basal temporal lobe (fusiform and inferior temporal); occipital lobe (lateral occipital, cuneus, and pericalcarine); and striatum (caudate and putamen).

In order to pool regional data across cohorts and tracers, SUVR values were standardized to z scores. The z scoring transformation was cohort-, radiotracer-, and region-specific and the reference groups consisted of CU participants of each study. We applied Gaussian Mixture Modeling to the regional data of each reference group to select the mean and SD of the left ("normal") Gaussian curve. These refined regional estimates were then used for z scoring the regional SUVR values (eFigure 1, links.lww.com/WNL/B861).

In addition, standardized quantification of global amyloid burden was obtained using the Centiloid (CL) scale.[22] PET scans from the ALFA, EMIF-AD, and ABIDE studies were processed by the Barcelonaβeta Brain Research Center (BBRC) using a validated standard CL pipeline.[23] CL values were directly obtained from the OASIS-3 and ADNI databases. As per standard guidelines, the reference region used for CL was the whole cerebellum for all data.[22]

SuStaIn Model

In this work, the Mixture SuStaIn implementation in PySuStaIn, cloned from the master branch on 30 October 2020, was used with Python 3.7. SuStaIn is a probabilistic machine learning algorithm that can characterize the heterogeneity of disease by inferring both patterns of disease progression (subtypes) and an individual's disease stage (i.e., degree of progression within a subtype) from cross-sectional data. The number of SuStaIn stages is defined by the number of biomarkers (in our case, ROIs) provided to the model. The model uses a data likelihood based on how far a biomarker measurement deviates from normality to group events based on their associated z score (e.g., 1, 2 , or 3 SDs away from control population mean) for each biomarker. However, in cases where the control population displays little abnormality (such as the case in our work, where amyloid load in the reference group will be low), the resulting z scores in patients can become too large in comparison. Instead, it is more sensible to use 2 distributions, one to describe the control population and a separate one to describe patients' measurements, therefore defining an event as a biomarker (in our case, regional SUVR of the 17 predefined ROIs) going from normal to abnormal (as in the event-based model[12,24]).

The SuStaIn model fitting consists of an iterative procedure that simultaneously optimizes subtype event sequences and subtype classification for a preselected number of subtypes. Model out-of-sample likelihoods across 10 folds were used to calculate the cross-validation information criterion (CVIC) per model. The CVIC is a measure of how well the model fits the test data, similar to the Akaike information criterion, but with less penalty on model complexity.[25] A complete mathematical description of the SuStaIn algorithm is available.[11] The number of subtypes was iteratively increased, and the model chosen for further analysis was selected based on the CVIC. In particular, we repeated the cross-validation analysis 20 times to exclude spurious findings and picked the subtype model such that the CVIC was lowest or, in cases where the

CVIC was very similar, had the lower model complexity (i.e., fewer subtypes).

Statistical Analyses

Statistical analyses were performed using Statistical Package for the Social Sciences (SPSS) version 26 and significance was set at $p < 0.05$.

Optimal Model Fit

The SuStaIn model was constructed based on the full baseline dataset (n = 3,010) and the optimal number of subtypes was tested by iteratively increasing the number of selected subtypes until the lowest CVIC value was reached. In addition, Spearman rank correlation analyses were used to assess the agreement between the regional ordering of a 1-trajectory model (i.e., 1 subtype, as per previously proposed staging models) and that of each of the subtypes determined by the optimal model. Rank correlations between subtypes were also determined.

Subtype Analyses

Overall differences between subtypes were assessed independently of stage. First, participants classified as stage 0 were labeled as no subtype and excluded from analyses. For participants assigned to stage ≥1, only those with a strong probability (>50%) of assignment to a subtype were included. A multinomial logistic regression (MLR) was used to determine the effect of demographics and risk factors on subtype assignment, such as age, cohort representation, male/female proportion, *APOE* ε4 and *APOE* ε2 carriers, Mini-Mental State Examination (MMSE) scores, and diagnostic groups. Next, 2 separate MLRs were used to determine the relationship between subtypes and biomarkers of AD pathology (amyloid and p-tau), corrected for the variables above. In addition to *z*-scored CSF p-tau, the first model included CL as a marker for amyloid pathology, while the second model included *z*-scored CSF $A\beta_{42}$. CSF values were *z* scored based on the mean and SD from the Gaussian mixture model–derived normal curve of each cohort. CSF was available for 1,522 participants (ABIDE: 241 [15.8%], ADNI: 858 [56.4%], ALFA+: 303 [19.9%], EMIF-AD: 120 [7.9%]).

Longitudinal Validation

The optimal SuStaIn model derived from the baseline data was subsequently applied to the subset (n = 591) of available longitudinal amyloid PET scans. Descriptive statistics were used to determine subtype stability (proportion of participants classified as the same subtype at follow-up) and stage progression (proportion of participants with lower, same, or higher stage at follow-up). In addition, an MLR was used to assess whether annualized rates of change in CL were different between subtypes, accounting for all significant covariates and baseline amyloid burden.

Data Availability

The data that support the findings of this study can be made available upon request from the study-specific principal investigator (i.e., ABIDE, EMIF-AD, ALFA) or are openly available (i.e., ADNI and OASIS open-source databases).

Results

The main demographics are shown in Table 1. Across cohorts, participants had a mean age of 68.72 ± 9.06 years and 51.8% were female. Most participants were CU (n = 1890 [62.4%]), MMSE score was 27.88 ± 2.93, and the proportion of *APOE* ε4 carriers was relatively high (42.1%).

Identified Subtypes of Amyloid Accumulation

The optimal model fit identified 3 different subtypes according to the CVIC (eFigures 2 and 3, links.lww.com/WNL/B861). The 3 subtypes are referred to as frontal, parietal, and occipital in the remainder of this study according to the earliest regions to become abnormal in each of them.

In the frontal subtype, the first abnormalities in amyloid PET signal were identified in the medial orbitofrontal region, progressing from the anterior to the posterior parts of the brain, and culminating with the involvement of the striatum and the occipital lobe. The parietal subtype also identified the striatum and occipital lobe as the last to become abnormal; the first regions to display abnormality were the posterior cingulate and the precuneus, with the intermediate spatial-temporal progression evolving from posterior to anterior regions. The occipital subtype displayed an inverse overall ordering, beginning in the occipital and temporal–parietal lobes, progressing to frontal regions, and ending in the striatum (Figure 1A and eFigure 4, links.lww.com/WNL/B861).

In comparison, the regional ordering from a 1-trajectory model closely resembled previously proposed staging models, with a medial frontal and precuneal start of amyloid accumulation, expanding throughout the cortex, and ending with the occipital cortex and striatum (Figure 1B). This regional ordering was strongly and positively correlated with the regional ordering of the frontal ($\rho = 0.90$, $p < 0.001$) and the parietal ($\rho = 0.89$, $p < 0.001$) subtypes, but not with the occipital subtype ($\rho = -0.01$, $p = 0.96$; eFigure 5, links.lww.com/WNL/B861). When comparing subtypes, the regional ordering of the frontal and parietal was positively correlated ($\rho = 0.74$, $p < 0.001$), while occipital subtype regional ordering did not significantly correlate with the frontal ($\rho = -0.18$, $p = 0.50$) or parietal subtypes ($\rho = -0.04$, $p = 0.88$; eFigure 6).

Subtype Assignment

Across the complete baseline dataset (n = 3,010), the majority of scans either showed fully normal (stage 0: n = 1810 [60.1%]) or widespread abnormal (stage 17: n = 282 [9.4%]) Aβ levels across all brain regions, which challenged accurate subtype assignment (Figure 2). Therefore, only cases with a strong subtype assignment probability (>50% probability) across stages higher than 0 were selected for subsequent subtype analyses (n = 788 [26.2%]). Within the 788 participants with strong subtype

Figure 1 Representation of the 3 Subtypes

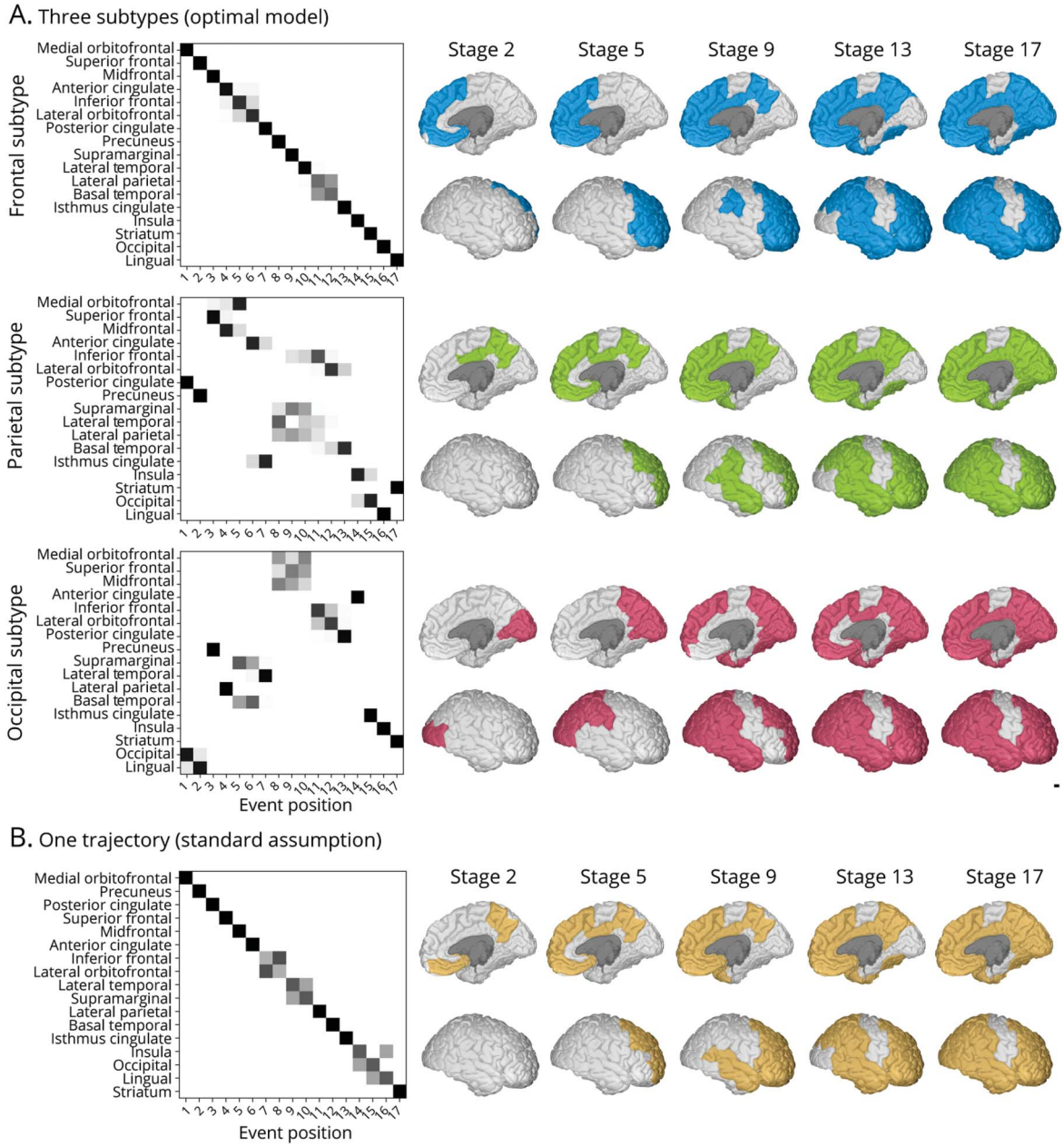

(A) Representation of the final 3 subtypes as identified by Subtype and Stage Inference (SuStaIn), referred to as frontal (top row), parietal (middle row), and occipital (bottom row), in accordance with the earliest regions to become abnormal. (B) The same representation for a 1-trajectory model across the dataset, which was not preferred against the 3-subtype model.

assignment, the majority (n = 415 [52.5%]) was assigned to the frontal, followed by the parietal (n = 199 [25.3%]) and occipital subtypes (n = 175 [22.2%]). This distribution was present within each cohort, with the exception of ABIDE (n = 101), where the majority of participants (n = 46 [45.5%]) were assigned to the parietal subtype instead ($\chi^2 = 70.31$, $p < 0.001$; Figure 3A and eTable 1, links.lww.com/WNL/B861).

Subtype Differences

Demographics per subtype can be found in Table 2. The male/female proportion was similar between subtypes. Participants assigned to the parietal subtype were younger compared to the frontal ($\beta = 0.05$, $p < 0.001$) and occipital ($\beta = 0.04$, $p = 0.005$). MMSE scores did not differ between subtypes, but diagnostic groups were differentially represented, with occipital displaying a higher proportion of participants with dementia than the other two (vs frontal: $\beta = 0.84$, $p < 0.001$; vs parietal: $\beta = 0.63$, $p = 0.02$; Figure 3B). The proportion of carriers across subtypes was similar for the ε2 allele (6.6%–7.9%), while ε4 carriership differed, with the highest percentage of *APOE* ε4 carriers observed in the frontal subtype (vs parietal: $\beta = -0.43$, $p = 0.02$; vs occipital: $\beta = -0.79$, $p < 0.001$; Figure 3C).

Figure 2 Subtype Assignment Probability Against Assigned Stage

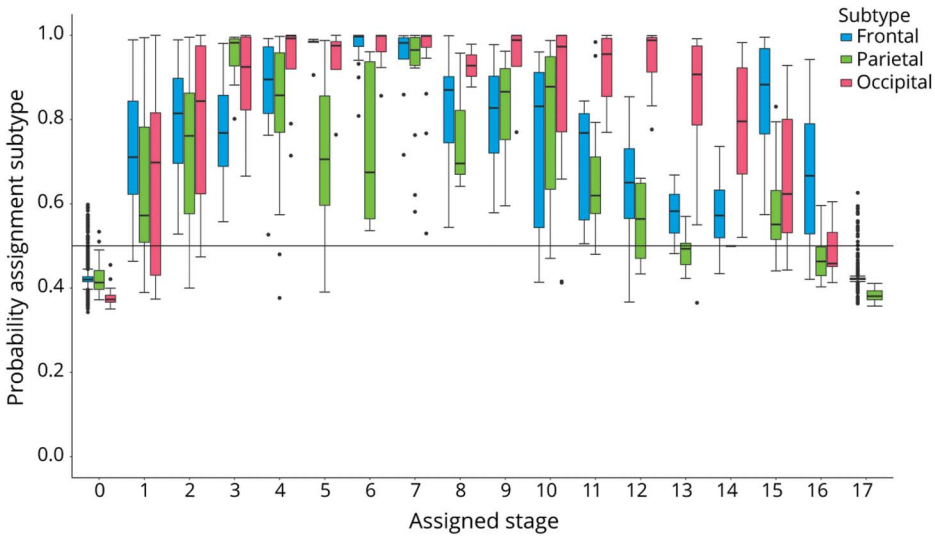

Boxplots show the relationship between stage assignment on the x-axis against the probability of subtype assignment on the y-axis for the whole baseline dataset. The solid line represents the cutoff for high probability, i.e., >50%. It can be appreciated that subtype assignment probability is lowest for those participants in stage 0 or 17, who present little least spatiotemporal information. Also, the highest probability assignment is observed for those participants around 7, where the subtypes are most different from each other.

With respect to the biomarkers of AD pathology, MLR analyses (n = 430) corrected for the variables above showed significantly higher amyloid burden as expressed in CL levels for the frontal subtype compared to the parietal ($\beta = -0.02$, $p = 0.002$) and occipital ($\beta = -0.01$, $p = 0.02$), but no differences for CSF $A\beta_{42}$ (Figure 3, D and E). CSF p-tau levels were also significantly higher for the frontal subtype compared to parietal (CL model: $\beta = -0.19$, $p = 0.006$; CSF $A\beta_{42}$ model: $\beta = -0.25$, $p < 0.001$) and occipital (CL model: $\beta = -0.10$, $p = 0.11$; CSF $A\beta_{42}$ model: $\beta = -0.14$, $p = 0.03$); parietal and occipital did not differ (Figure 3F).

Longitudinal Validation

A total of 519 (ADNI, n = 376 [72.4%]; OASIS, n = 143 [27.6%]) participants had available longitudinal amyloid PET at least 4 years after baseline available (mean 5.5 ± 1.2 years [4.0–9.6]). Mean follow-up time was longer for OASIS (mean 6.2 ± 1.4 years [4.0–9.6]) compared to ADNI (mean 5.2 ± 1.0 years [4.0–9.4], $F = 71.0$, $p < 0.001$). Participants with longitudinal PET data had highly similar demographics compared to the full cohort, with most participants CU at baseline (n = 320 [61.7%]), mean MMSE score 28.72 (SD 1.61), average age 70.0 years (SD 9.01), and 51.3% female.

The longitudinal validation was performed across the entire sample (even if the baseline probability of subtype assignment was lower than 50%). In the complete longitudinal sample, the majority of participants were assigned to "no subtype" (i.e., stage 0) at baseline (n = 381 [73.4%]), followed by frontal subtype (n = 86 [16.6%]), parietal (n = 47 [9.1%]), and occipital (n = 5 [1.0%]).

Subtype Stability

In the entire longitudinal sample, 421 (81.1%) participants were stable in subtype assignment; 322 remained stage 0, (i.e., "no subtype") 65 from the frontal, and 34 from the parietal subtype. In contrast, 98 (18.9%) participants changed subtype assignment at follow-up ("no subtype," 59; frontal, 21; parietal, 13; and occipital, 5 at baseline). From those, frontal mostly changed to parietal and vice-versa (F→P: 76.2% [n = 16] and F→0: 23.8% [n = 5]; P→F: 76.9% [n = 10] and P→O: 7.7% [n = 1]), while all occipital participants (n = 4) changed subtype, mostly to parietal (O→F: 20.0% [n = 1] and O→P: 60.0% [n = 3]; Figure 4A). The most common change in subtype occurred in participants who started in stage 0 (0→F: 66.1% [n = 39], 0→P: 30.5% [n = 18], 0→O: 3.4% [n = 2]; Figure 4B).

Amyloid Accumulation

When we evaluated staging, we found that 69.0% (n = 358) remained stable, 25.6% (n = 133) progressed to later stages, and 5.4% (n = 28) of participants regressed in stage at follow-up. This was independent of subtype stability. These changes in stage can also be observed using the CL scale (Figure 4C). Yearly rates of change in CL were different between participants assigned to 1 of the 3 subtypes or "no subtype" at baseline, even after accounting for syndromic diagnosis, cohort, *APOE* ε4 carriership, and baseline amyloid burden. More specifically, the longitudinal rates of change were lower for no subtype (vs frontal: $\beta = 4.09$, $p < 0.001$; vs parietal: $\beta = 4.23$, $p < 0.001$; vs occipital: $\beta = 2.84$, $p = 0.004$) and slightly higher for occipital subtype (vs frontal: $\beta = -0.08$, $p < 0.001$; vs parietal: $\beta = -0.07$, $p = 0.03$; vs no subtype: $\beta = -0.35$, $p < 0.001$), but did not differ between the frontal and parietal subtypes.

Discussion

In this work, applying the SuStaIn model to a pooled dataset of >3000 PET scans provided support for the existence of 3

Figure 3 Cross-sectional Relationships

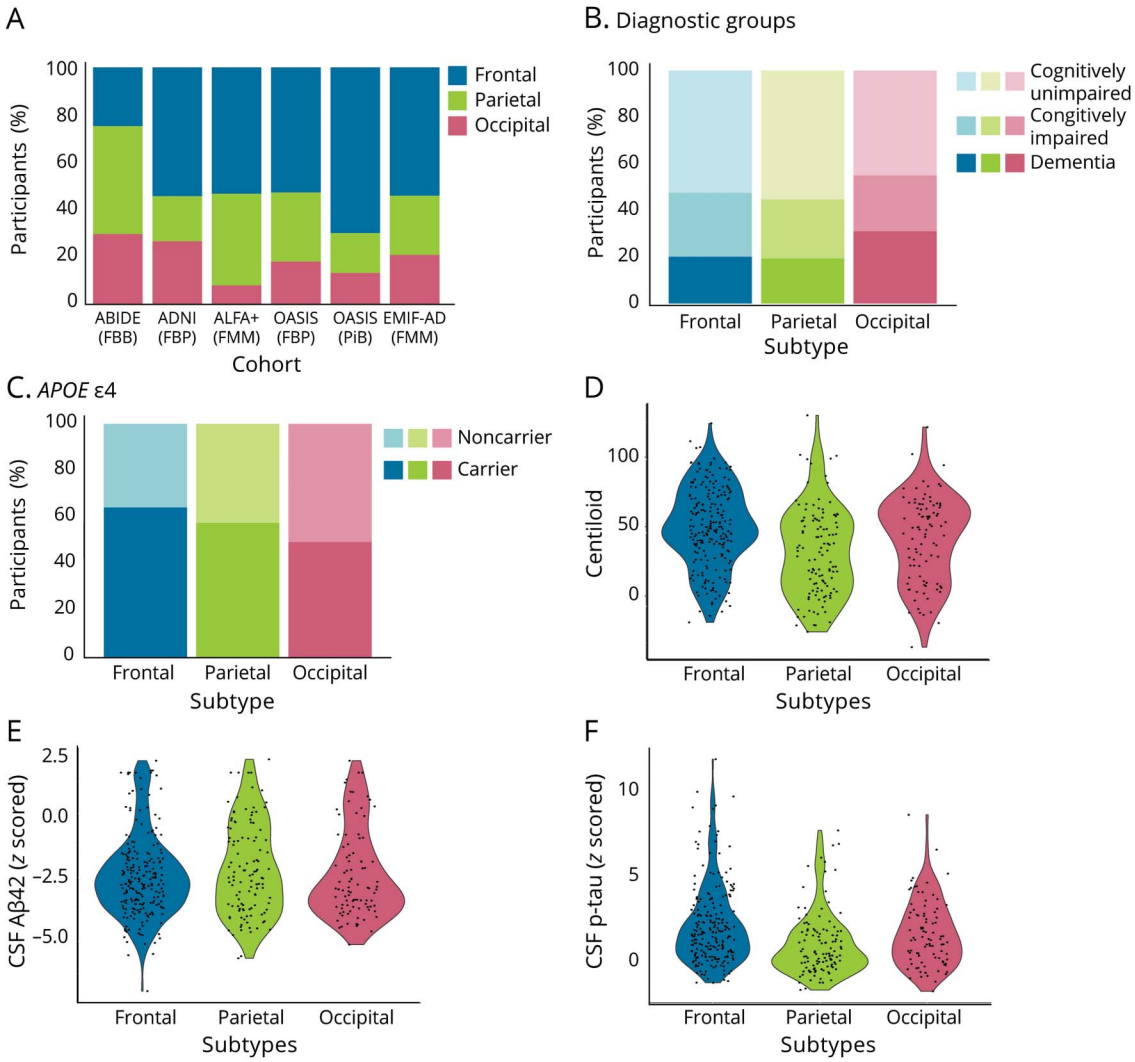

For the 788 participants with a strong subtype assignment (>50% probability) at baseline, differences in subtypes are shown for (A) cohort and tracer representation, (B) diagnostic groups, (C) *APOE* ε4 carriership, (D) amyloid burden expressed in Centiloid units, (E) amyloid burden in CSF $A\beta_{42}$, and (F) CSF p-tau. Demographics and risk factors (A–C) were significantly different between the 3 subtypes. (D, F) The frontal subtype was associated with higher Centiloid and CSF p-tau values, although (E) no differences were observed for CSF $A\beta_{42}$ between subtypes. ABIDE = Alzheimer's biomarkers in daily practice project; ADNI = Alzheimer's Disease Neuroimaging Initiative; ALFA = Alzheimer's and Family cohort of the BarcelonaBeta Brain Research Center; EMIF-AD = European Medical Information Framework for AD; FBB = [^{18}F]florbetaben; FBP = [^{18}F]florbetapir; FMM = [^{18}F]flutemetamol; OASIS = Open Access Series of Imaging Studies; PiB = Pittsburgh compound B.

subtypes of topographic cortical amyloid accumulation, in contrast to the traditional assumption of single-trajectory models reported previously.[4,6,8,9] The 3 subtypes are referred to as frontal, parietal, and occipital based on the earliest regions to show abnormality. Of these, the frontal subtype was most prevalent in our sample and was associated with a higher proportion of *APOE* ε4 carriership and higher amyloid and tau burden, whereas the parietal subtype was associated with younger age. The occipital subtype showed a higher proportion of patients with dementia.

Previous models of amyloid accumulation in AD were based on the assumption of a universal trajectory of disease progression, consistently implicating the medial cortical regions early in the process of Aβ accumulation, followed by cortical association areas, and finally the late involvement of occipital and striatal regions.[6-9] This population-level ordering was also identified by SuStaIn when the model was set to recover one trajectory, which seems to correspond to an average of the most common frontal and parietal subtypes (eFigure 2, links.lww.com/WNL/B861). We now extend on former studies, as SuStaIn was able to further resolve subtype-specific initial stages, identifying the orbitofrontal cortex and precuneus regions as the starting point of distinct subtypes. We observed that the concomitant abnormality in those regions corresponded to an intermediate SuStaIn stage shared between the frontal and parietal subtypes instead (i.e., ~stage 8, Figure 1). The precuneus seems more strongly implicated in patients with early-onset AD.[26] The parietal subtype was more often observed in the ABIDE clinical cohort from the Alzheimer

Figure 4 Longitudinal Validation

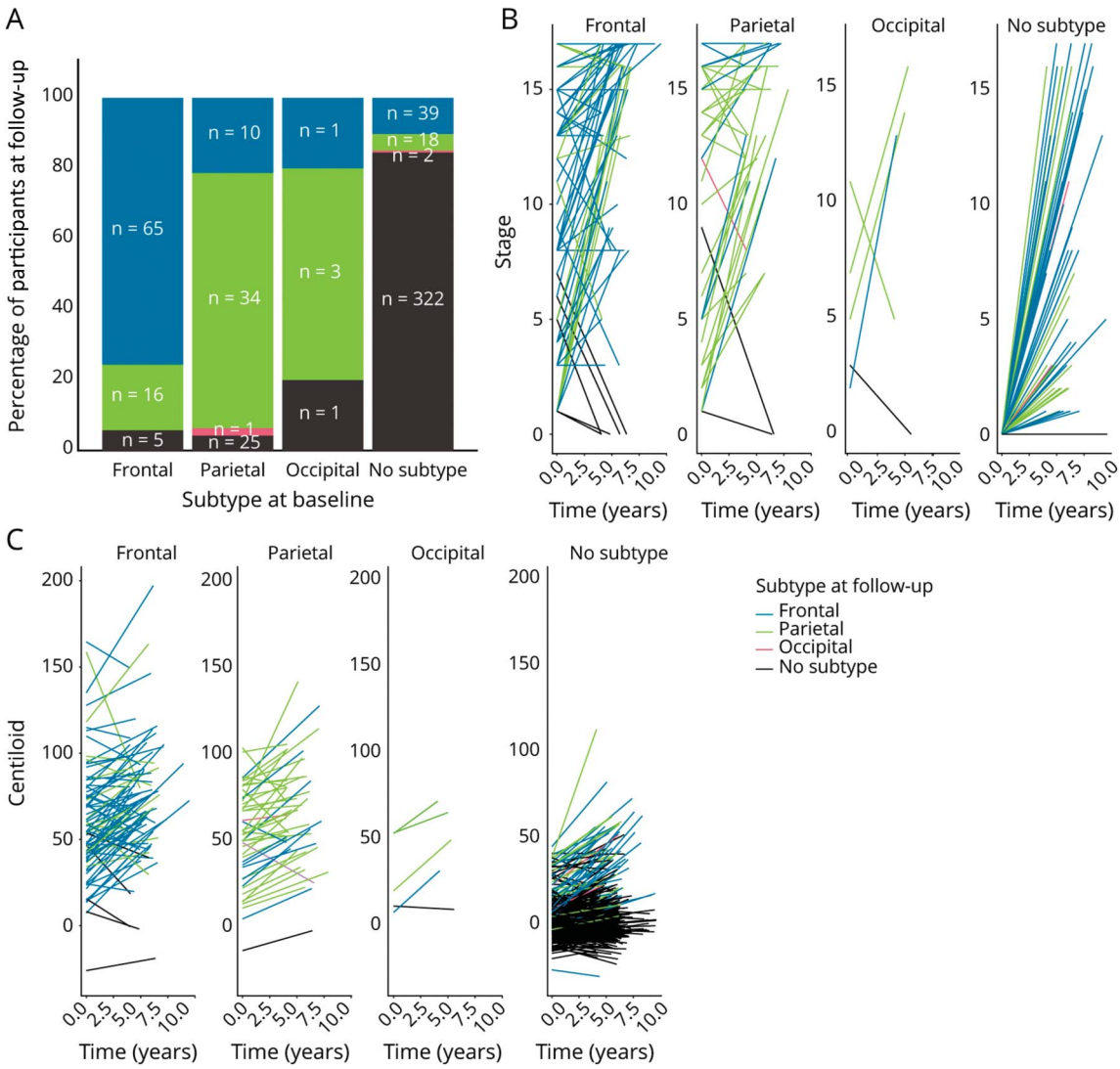

(A) Subtype assignment at baseline vs at follow-up. Spaghetti plots illustrate the change in (B) stage and (C) Centiloid units per subtype as assigned at baseline. Lines are color coded to show changes in subtype assignment at follow-up. Overall, changes in stage are associated with changes in Centiloid and yearly rates of change were lowest for the frontal subtype.

Center Amsterdam, a tertiary referral center specialized in dementia at a young age.[16,27]

In the absence of neuropathologic confirmation, it is important to note that recent work on regional visual assessment of [^{18}F]flutemetamol PET images supports these results.[28] The expert visual assessment of almost 500 amyloid-PET images showed both the traditional joint and early involvement of the medial orbitofrontal cortex and precuneus, as well as a non-negligible proportion of CU participants displaying isolated amyloid burden, specifically in one of these regions.[28] The occipital lobe is not part of the visual read guidelines of amyloid PET images,[28] limiting the available information on the incidence of occipital uptake. Nonetheless, a subset of participants in this previous report did show a relatively early involvement of temporal regions, especially together with parietal ones—a pattern that could reflect the first half of the occipital subtype progression (up to ~stage 9, Figure 1).

The identification of the occipital subtype by SuStaIn is remarkably distinct from traditional reports of early amyloid deposition in AD. In fact, the occipital lobe is commonly assumed to only harbor amyloid pathology towards the end of the disease process.[6,8,9] Nonetheless, posterior or occipital uptake is often attributed to cerebral amyloid angiopathy (CAA), which most commonly affects this region and is a known risk factor for AD.[29] Under this hypothesis, the assignment of participants to the occipital subtype could suggest the identification of CAA as cerebral Aβ accumulation by SuStaIn. Nonetheless, there is neuropathologic support for an alternative hypothesis, i.e., that the occipital signal actually reflects cortical amyloid pathology. More specifically, Braak

Table 2 Baseline Demographics for Each Subtype

	Frontal (n = 414)[a]	Parietal (n = 199)[b]	Occipital (n = 175)[c]
Age, y	72.12 (8.14)	69.26 (9.61)	72.13 (8.07)
Sex, F	196 (47.3)	97 (43.7)	85 (48.6)
MMSE	27.35 (3.19)	27.40 (2.56)	26.56 (3.50)
***APOE* ε4 carriership+[d]**	264 (64.2)	113 (57.7)	86 (49.4)
***APOE* ε2 carriership+[e]**	31 (7.5)	13 (6.6)	12 (6.9)
Centiloid	50.73 (27.52)	36.71 (28.99)	40.65 (29.26)
***z*-scored CSF $A\beta_{42}$**	−2.45 (1.60)	−2.19 (1.78)	−2.38 (1.72)
***z*-scored CSF p-tau**	2.08 (2.501)	0.91 (2.03)	1.51 (2.03)

Abbreviations: Aβ = β-amyloid; AD = Alzheimer disease; CU = cognitively unimpaired, including both controls and subjective cognitive decliners. Cognitively impaired participants had a clinical diagnosis of mild cognitive impairment or a Clinical Dementia Rating of 0.5 (in the absence of a clinical diagnosis). Dementia includes both AD and non-AD. Values are mean (SD) or n (%).
[a] 2 (0.5%) missing, 215 (51.9%) CU, 112 (27.1%) cognitively impaired, 82 (19.8%) dementia.
[b] 2 (1.0%) missing, 109 (54.8%) CU, 50 (25.1%) cognitively impaired, 38 (19.1%) dementia.
[c] 4 (2.3%) missing, 77 (44.0%) CU, 41 (23.4%) cognitively impaired, 53 (30.3%) dementia.
[d] Participant carries at least 1 *APOE* ε4 allele.
[e] Participant carries at least 1 *APOE* ε2 allele.

and Braak[5] described basal occipital uptake as part of the first neuropathologic stage in AD. Also, (posterior) amyloid burden is observed in approximately 50% of patients with dementia with Lewy bodies (DLB), which is suggested to reflect AD copathology and is associated with a worse prognosis.[30] A post hoc analysis of subtype classification in specifically the clinical ABIDE cohort provides further support of this observation, as the occipital subtype was overrepresented in the DLB patient population (eFigure 7, links.lww.com/WNL/B861). To further determine the underlying pathology of this subtype, its relationship to (occipital) microbleeds (a symptom of CAA[29]) and different etiologies in patients with non-AD dementia should be investigated. Still, this overrepresentation of participants with dementia in the occipital subtype indicates that early amyloid-PET signal in the occipital lobe may harbor relevant prognostic information. As such, future AD research should consider the assessment of occipital regions, and future visual read guidelines could consider including the occipital lobe for the assessment of amyloid PET scans should these findings be confirmed.

Overall, subtype assignment might have the highest utility in the predementia stages of AD, considering the main differences between the trajectories are apparent at the beginning of the process. Indeed, the highest probability of subtype assignment was observed in individuals at the early to intermediate stages of amyloid-PET abnormality (stages 6–7), while higher stages resulted in lower probability of assignment as subtypes merge into similar trajectories (Figure 2). Nonetheless, the earliest regions of each subtype still display higher amyloid at the late stages, indicating that subtypes can still be identified even beyond the amyloid saturation point. While this suggests that the subtypes are not merely ephemeral states, an important question is whether they have prognostic value, both in terms of differences in speed of amyloid accumulation as well as in terms of risk or speed of subsequent pathologic progress and cognitive decline. Regarding the former, our longitudinal analyses already suggest the frontal subtype to have lower amyloid accumulation rates compared to the other groups. However, these results must be interpreted with caution, as the sample sizes of both parietal and occipital subtypes were too small. Another possible effect of amyloid subtypes could be related to subsequent tau spread. Whereas previous literature suggests tau spread beyond the medial temporal lobe to only occur after sufficient amyloid deposition, it remains unclear whether and how the spatial distribution of amyloid further influences this event. In addition, recent work identified 4 subtypes of tau accumulation, further suggesting a possible interaction between amyloid and tau spatial-temporal trajectories.[13] In terms of cognition, the different proportions of clinical diagnostic groups (i.e., CU, cognitively impaired, and dementia) already indicate worse prognosis for the occipital subtype. Nonetheless, clinical diagnosis is a relatively crude measure for overall cognitive performance, and further exploration of the severity and type of cognitive symptoms associated with each of the subtypes will be necessary to determine their clinical relevance. In addition, previous work has shown that the extent of amyloid burden as measured in CL units predicts the risk of global cognitive decline.[31] Future work should investigate whether additional information on amyloid accumulation subtype further improves risk stratification.

There are some methodologic limitations to consider when interpreting the results of this work. First, while SuStaIn uses a cross-validation framework and the results are bootstrapped, one could argue we should have used a separate training and test set to validate the results. We opted not to do this because

the majority of participants were cognitively normal and had no amyloid, thus the amount of data with variable amyloid burden was already limited. In addition, it should be noted that the majority of the data included in this work were used previously to describe a 1-trajectory amyloid accumulation pattern, although implementing a different methodologic approach.[9] Thus, the high agreement between the SuStaIn-identified 1-trajectory model and some of the previous staging work is possibly partly due to the reuse of data. Second, while CL units are generally used to pool PET data, we standardized regional SUVR using a *z*-scoring approach. This was done to account for not only tracer differences, but also for the differential signal distortion effects between medial and lateral regions (inherit to the PET metric),[4] which is not taken into account in the CL approach.[22] Third, whereas our initial results suggest robust assignment over time (i.e., stable for 87.7% of participants), only ADNI and OASIS-3 had available longitudinal PET imaging data, limiting our sample sizes for longitudinal analyses, especially for the occipital subtype. Finally, yearly rates of change in amyloid burden might be underestimated for the occipital subtype, as the CL mask does not include this region.

The SuStaIn model provides data-driven evidence for the existence of 3 spatiotemporal subtypes of cortical amyloid accumulation and opens possibilities for further exploration of the identified subtypes. The initial results indicate differences in their relation to AD risk factors as well as prognosis, and therefore suggest that subtype assignment may have clinical relevance or could support individualized risk assessment. Future work should assess whether subtypes are associated with distinct cognitive profiles or risk of cognitive decline and investigate the possible underlying pathophysiology.

Acknowledgment

The data used in this article are part of the Alzheimer's and Family cohort of the Barcelonaβeta Brain Research Center (ALFA) study. The authors thank the ALFA project participants as well as the ALFA collaborators: Annabella Beteta, Anna Brugulat, Raffaele Cacciaglia, Alba Cañas, Carme Deulofeu, Irene Cumplido, Ruth Dominguez, Maria Emilio, Karine Fauria, Sherezade Fuentes, Laura Hernandez, Gema Huesa, Jordi Huguet, Paula Marne, Tania Menchón, Albina Polo, Sandra Pradas, Blanca Rodriguez-Fernandez, Aleix Sala-Vila, Gonzalo Sánchez-Benavides, Gemma Salvadó, Anna Soteras, and Marc Vilanova.

Study Funding

The project leading to this article has received funding from the Innovative Medicines Initiative 2 Joint Undertaking under grant agreement 115952. This Joint Undertaking receives support from the European Union's Horizon 2020 research and innovation programme and EFPIA. This communication reflects the views of the authors and neither the Innovative Medicines Initiative nor the European Union or EFPIA are liable for any use of the information contained herein. The ALFA study received funding from "la Caixa" Foundation (ID 100010434) under agreement LCF/PR/GN17/50300004, the Alzheimer's Association, and an international anonymous charity foundation through the TriBEKa Imaging Platform project (TriBEKa-17-519007). Additional support has been received from the Universities and Research Secretariat, Ministry of Business and Knowledge of the Catalan Government under grant 2017-SGR-892. J.D.G. is supported by the Spanish Ministry of Science and Innovation (RYC-2013-13054) and the Agencia Estatal de Investigación Proyectos de I+D+i Retos Investigación (RTI2018-102261-B-I00).

Disclosure

L.E. Collij, G. Salvadó, V. Wottschel, S.E. Mastenbroek, P. Schoenmakers, F. Heeman, L. Aksman, A.M. Wink, B.N.M. van Berckel, and W.M. van der Flier report no disclosures relevant to the manuscript. P. Scheltens received grants from GE Healthcare, Piramal, and Merck, paid to his institution, and has received speaker's fees paid to his institution from Alzheimer Center, VU University Medical Center, Lilly, GE Healthcare, and Roche. P.J. Visser has served as a member of the advisory board of Roche Diagnostics and received nonfinancial support from GE Healthcare, research support from Biogen, and grants from Bristol-Myers Squibb, EU/EFPIA Innovative Medicines Initiative Joint Undertaking, and EU Joint Programme–Neurodegenerative Disease Research (JPND and ZonMw). F. Barkhof received payment and honoraria from Bayer Genzyme, Biogen-Idec, TEVA, Merck, Novartis, Roche, IXICO Ltd., GeNeuro, and Apitope Ltd. for consulting; payment from IXICO Ltd. and Medscape for educational presentations; and research support via grants from the EU/EFPIA Innovative Medicines Initiative Joint Undertaking (AMYPAD consortium), EuroPOND (H2020), UK MS Society, Dutch MS Society, PICTURE (IMDI-NWO), NIHR UCLH Biomedical Research Centre (BRC), and ECTRIMS-MAGNIMS. S. Haller is a member of the EPAD Imaging SAG, consultant for Spineart, consultant for WYSS, and speaker for GE Healthcare. J.D. Gispert has received speaker's fees from Biogen and Philips; holds a Ramón y Cajal fellowship (RYC-2013-13054); and has received research support from the EU/EFPIA Innovative Medicines Initiative Joint Undertaking AMYPAD grant agreement 115952 and from Ministerio de Ciencia y Universidades (grant agreement RTI2018-102261). I. Lopes Alves reports no disclosures relevant to the manuscript. Go to Neurology.org/N for full disclosures.

Publication History

Received by *Neurology* May 26, 2021. Accepted in final form January 18, 2022.

Appendix 1 Authors

Name	Location	Contribution
Lyduine E. Collij, PhD	Amsterdam UMC, VUmc, the Netherlands	Literature search, design, data collection, analysis, interpretation, drafted manuscript

Appendix 1 *(continued)*

Name	Location	Contribution
Gemma Salvadó, PhD	BarcelonaBeta Research Center, Barcelona, Spain	Literature search, design, data collection, analysis, interpretation, drafted manuscript
Viktor Wottschel, PhD	Amsterdam UMC, VUmc, the Netherlands	Design, analysis, interpretation, drafted manuscript, revised manuscript
Sophie E. Mastenbroek, MSc	Amsterdam UMC, VUmc, the Netherlands	Analyses, interpretation, drafted manuscript, revised manuscript
Pierre Schoenmakers, BSc	Amsterdam UMC, VUmc, the Netherlands	Data collection, analysis, revised manuscript
Fiona Heeman, MSc	Amsterdam UMC, VUmc, the Netherlands	Data collection, interpretation, revised manuscript
Leon M. Aksman, PhD	Stevens Neuroimaging and Informatics Institute, University of Southern California, Los Angeles	Analysis, revised manuscript
Alle Meije Wink, PhD	Amsterdam UMC, VUmc, the Netherlands	Interpretation, revised manuscript
Bart N.M. van Berckel, PhD	Amsterdam UMC, VUmc, the Netherlands	Data collection, interpretation, revised manuscript
Wiesje M. van der Flier, PhD	Amsterdam UMC, VUmc, the Netherlands	Data collection, analyses, interpretation, revised manuscript
Philip Scheltens, PhD	Amsterdam UMC, VUmc, the Netherlands	Data collection, revised manuscript
Pieter Jelle Visser, PhD	Amsterdam UMC, VUmc, the Netherlands	Data collection, revised manuscript
Frederik Barkhof, PhD	Amsterdam UMC, VUmc, the Netherlands; University College London, UK	Data collection, interpretation, revised manuscript
Sven Haller, PhD	Faculty of Medicine of the University of Geneva, Switzerland	Design, analyses, interpretation, revised manuscript
Juan Domingo Gispert, PhD	BarcelonaBeta Research Center, Barcelona, Spain	Design, data collection, analyses, interpretation, revised manuscript
Isadora Lopes Alves, PhD	Amsterdam UMC, VUmc, the Netherlands	Literature search, design, analysis, interpretation, drafted manuscript

Appendix 2 Coinvestigators

ADNI coinvestigators are listed at links.lww.com/WNL/B862

Appendix 3 Coinvestigators

ALFA coinvestigators are listed at links.lww.com/WNL/B863

References

1. Salloway S, Gamez JE, Singh U, et al. Performance of [(18)F]flutemetamol amyloid imaging against the neuritic plaque component of CERAD and the current (2012) NIA-AA recommendations for the neuropathologic diagnosis of Alzheimer's disease. *Alzheimers Dement.* 2017;9:25-34.
2. Sabri O, Sabbagh MN, Seibyl J, et al. Florbetaben PET imaging to detect amyloid beta plaques in Alzheimer's disease: phase 3 study. *Alzheimers Dement.* 2015;11(8):964-974.
3. Clark CM, Schneider JA, Bedell BJ, et al. Use of florbetapir-PET for imaging β-amyloid pathology. *JAMA.* 2011;305(3):275-283.
4. Fantoni E, Collij L, Alves IL, Buckley C, Farrar G. The spatial–temporal ordering of amyloid pathology and opportunities for PET imaging. *J Nucl Med.* 2020;61(2):166-171.
5. Braak H, Braak E. Neuropathological stageing of Alzheimer-related changes. *Acta Neuropathol.* 1991;82(4):239-259.
6. Grothe MJ, Barthel H, Sepulcre J, et al. In vivo staging of regional amyloid deposition. *Neurology.* 2017;1489(20):2031-2038.
7. Hanseeuw BJ, Betensky RA, Mormino EC, et al. PET staging of amyloidosis using striatum. *Alzheimers Dement.* 2018;14(10):1281-1292.
8. Mattsson N, Palmqvist S, Stomrud E, Vogel J, Hansson O. Staging β-amyloid pathology with amyloid positron emission tomography. *JAMA Neurol.* 2019;76(11):1319-1329.
9. Collij LE, Heeman F, Salvado G, et al. Multitracer model for staging cortical amyloid deposition using PET imaging. *Neurology.* 2020;95(11):e1538–e1553.
10. Ossenkoppele R, Schonhaut DR, Scholl M, et al. Tau PET patterns mirror clinical and neuroanatomical variability in Alzheimer's disease. *Brain.* 2016;139(Pt 5):1551-1567.
11. Young AL, Marinescu RV, Oxtoby NP, et al. Uncovering the heterogeneity and temporal complexity of neurodegenerative diseases with Subtype and Stage Inference. *Nat Commun.* 2018;9(1):4273.
12. Young AL, Oxtoby NP, Daga P, et al. A data-driven model of biomarker changes in sporadic Alzheimer's disease. *Brain.* 2014;137(Pt 9):2564-2577.
13. Vogel JW, Young AL, Oxtoby NP, et al. Four distinct trajectories of tau deposition identified in Alzheimer's disease. *Nat Med.* 2021;27(5):871-881.
14. Molinuevo JL, Gramunt N, Gispert JD, et al. The ALFA project: a research platform to identify early pathophysiological features of Alzheimer's disease. *Alzheimers Dement.* 2016;2(2):82-92.
15. Konijnenberg E, Carter SF, Ten Kate M, et al. The EMIF-AD PreclinAD study: study design and baseline cohort overview. *Alzheimers Res Ther.* 2018;10(1):75.
16. de Wilde A, van Maurik IS, Kunneman M, et al. Alzheimer's biomarkers in daily practice (ABIDE) project: rationale and design. *Alzheimers Dement.* 2017;6:143-151.
17. LaMontagne PJ, Benzinger TLS, Morris JC, et al. OASIS-3: Longitudinal neuroimaging, clinical, and cognitively dataset for normal aging and Alzheimer's disease. *AAIC 2018 poster presentation* 2018;14(7):P1097.
18. Heeman F, Yaqub M, Lopes Alves I, et al. Optimized dual-time-window protocols for quantitative [(18)F]flutemetamol and [(18)F]florbetaben PET studies. *EJNMMI Res.* 2019;9(1):32.
19. Collij L, Konijnenberg E, Reimand J, et al. Assessing amyloid pathology in cognitively normal subjects using [(18)F]flutemetamol PET: comparing visual reads and quantitative methods. *J Nucl Med.* 2019;60(4):541-547.
20. Su Y, D'Angelo GM, Vlassenko AG, et al. Quantitative analysis of PiB-PET with FreeSurfer ROIs. *PLoS One.* 2013;8(11):e73377.
21. Desikan RS, Segonne F, Fischl B, et al. An automated labeling system for subdividing the human cerebral cortex on MRI scans into gyral based regions of interest. *Neuroimage.* 2006;31(3):968-980.
22. Klunk WE, Koeppe RA, Price JC, et al. The Centiloid Project: standardizing quantitative amyloid plaque estimation by PET. *Alzheimers Dement.* 2015;11(1):1-15.e14.
23. Salvado G, Molinuevo JL, Brugulat-Serrat A, et al. Centiloid cut-off values for optimal agreement between PET and CSF core AD biomarkers. *Alzheimers Res Ther.* 2019;11(1):27.
24. Fonteijn HM, Modat M, Clarkson MJ, et al. An event-based model for disease progression and its application in familial Alzheimer's disease and Huntington's disease. *Neuroimage.* 2012;60(3):1880-1889.
25. Reiss PT, Huang L, Cavanaugh JE, Roy AK. Resampling-based information criteria for best-subset regression. *Ann Inst Stat Math.* 2012;64(6):1161-1186.
26. Ossenkoppele R, Zwan MD, Tolboom N, et al. Amyloid burden and metabolic function in early-onset Alzheimer's disease: parietal lobe involvement. *Brain.* 2012;135(Pt 7):2115-2125.
27. van der Flier WM, Scheltens P. Amsterdam dementia cohort: performing research to optimize care. *J Alzheimers Dis.* 2018;62(3):1091-1111.
28. Collij LE, Salvado G, Shekari M, et al. Visual assessment of [(18)F]flutemetamol PET images can detect early amyloid pathology and grade its extent. *Eur J Nucl Med Mol Imaging.* 2021;48(7):2169-2182.
29. Charidimou A, Farid K, Tsai HH, Tsai LK, Yen RF, Baron JC. Amyloid-PET burden and regional distribution in cerebral amyloid angiopathy: a systematic review and meta-analysis of biomarker performance. *J Neurol Neurosurg Psychiatry.* 2018;89(4):410-417.
30. Chetelat G, Arbizu J, Barthel H, et al. Amyloid-PET and (18)F-FDG-PET in the diagnostic investigation of Alzheimer's disease and other dementias. *Lancet Neurol.* 2020;19(11):951-962.
31. van der Kall LM, Truong T, Burnham SC, et al. Association of beta-amyloid level, clinical progression and longitudinal cognitive change in normal older individuals. *Neurology.* 2021;96(5):e662–e670.

Published Ahead of Print on September 30, 2022 as 10.1212/WNL.0000000000201144

Neurology®

The most widely read and highly cited peer-reviewed neurology journal
The Official Journal of the American Academy of Neurology

AMERICAN ACADEMY OF NEUROLOGY®

Neurology Publish Ahead of Print
DOI: 10.1212/WNL.0000000000201144

CORRECTION

Spatial-Temporal Patterns of β-Amyloid Accumulation: A Subtype and Stage Inference Model Analysis

In the Research Article "Spatial-Temporal Patterns of β-Amyloid Accumulation: A Subtype and Stage Inference Model Analysis" by Collij et al.[1], the following information was mistakenly omitted from the Acknowledgements section:

> "Data were provided by OASIS OASIS-3: Principal Investigators: T. Benzinger, D. Marcus, J. Morris; NIH P50 AG00561, P30 NS09857781, P01 AG026276, P01 AG003991, R01 AG043434, UL1 TR000448, R01 EB009352. AV-45 doses were provided by Avid Radiopharmaceuticals, a wholly owned subsidiary of Eli Lilly. OASIS-3: https://doi.org/10.1101/2019.12.13.19014902."

The authors regret the omission.

REFERENCE

[1]Collij L, Salvadó G, Wottschel V, et al. Spatial-Temporal Patterns of β-Amyloid Accumulation: A Subtype and Stage Inference Model Analysis. *Neurology* 2022;98:e1692–e1703.